Simulation of the Earth's radiation budget by the European Centre for Medium-Range Weather Forecasts 40-year reanalysis (ERA40)

Richard P. Allan,[1] Mark A. Ringer,[2] J. Alison Pamment,[3] and Anthony Slingo[1]

Received 25 March 2004; revised 16 June 2004; accepted 29 June 2004; published 18 September 2004.

[1] The radiation budget simulated by the European Centre for Medium-Range Weather Forecasts (ECMWF) 40-year reanalysis (ERA40) is evaluated for the period 1979–2001 using independent satellite data and additional model data. This provides information on the quality of the radiation products and indirect evaluation of other aspects of the climate produced by ERA40. The climatology of clear-sky outgoing longwave radiation (OLR) is well captured by ERA40. Underestimations of about 10 W m^{-2} in clear-sky OLR over tropical convective regions by ERA40 compared to satellite data are substantially reduced when the satellite sampling is taken into account. The climatology of column-integrated water vapor is well simulated by ERA40 compared to satellite data over the ocean, indicating that the simulation of downward clear-sky longwave fluxes at the surface is likely to be good. Clear-sky absorbed solar radiation (ASR) and clear-sky OLR are overestimated by ERA40 over north Africa and high-latitude land regions. The observed interannual changes in low-latitude means are not well reproduced. Using ERA40 to analyze trends and climate feedbacks globally is therefore not recommended. The all-sky radiation budget is poorly simulated by ERA40. OLR is overestimated by around 10 W m^{-2} over much of the globe. ASR is underestimated by around 30 W m^{-2} over tropical ocean regions. Away from marine stratocumulus regions, where cloud fraction is underestimated by ERA40, the poor radiation simulation by ERA40 appears to be related to inaccurate radiative properties of cloud rather than inaccurate cloud distributions. *INDEX TERMS:* 1610 Global Change: Atmosphere (0315, 0325); 1833 Hydrology: Hydroclimatology; 3360 Meteorology and Atmospheric Dynamics: Remote sensing; 3359 Meteorology and Atmospheric Dynamics: Radiative processes; 3309 Meteorology and Atmospheric Dynamics: Climatology (1620); *KEYWORDS:* reanalysis, radiation budget, water vapor

Citation: Allan, R. P., M. A. Ringer, J. A. Pamment, and A. Slingo (2004), Simulation of the Earth's radiation budget by the European Centre for Medium-Range Weather Forecasts 40-year reanalysis (ERA40), *J. Geophys. Res.*, *109*, D18107, doi:10.1029/2004JD004816.

1. Introduction

[2] The interaction between atmospheric moisture, the radiation budget, and the large-scale circulation is fundamental in determining climate and its variability [e.g., *Hartmann et al.*, 2001]. The representation and improvement of these processes in numerical models requires careful analysis of high-quality observations of the Earth-atmosphere system. However, evaluation of the model simulations is limited by the paucity of these measurements. Reanalyses potentially address this limitation by enhancing the existing network of observations through a self-consistent data assimilation system. Further, the ability to provide detailed coverage of the present-day climate in the context of the synoptic situation has been demonstrated to be a powerful means of understanding the subtle processes important for determining the climate state and its variability [e.g., *Bony et al.*, 2004].

[3] The degree to which errors are introduced into the reanalysis through inaccurate observations, deficient model parameterizations or aspects of the assimilation system itself are not fully understood [e.g., *Trenberth et al.*, 2001]. Careful evaluation of these products is therefore required to ascertain their overall quality and to identify particular strengths and weaknesses of aspects of the simulated climate. One such component of reanalyses that may be readily evaluated is the radiative energy budget. The benefit of such an assessment is twofold. First, the radiative energy balance is a fundamental determinant of climate forcings and feedback and is therefore an important component of numerical weather prediction and climate models. Thus the potential applications for radiative fluxes and heating rates simulated by reanalyses are considerable. Second, radiative fluxes provide a wealth of diagnostic information pertaining

[1]Environmental Systems Science Centre, University of Reading, Reading, UK.
[2]Hadley Centre, Met Office, Exeter, UK.
[3]British Atmospheric Data Centre, Rutherford Appleton Laboratory, Chilton, UK.

0148-0227/04/2004JD004816$09.00

to the atmosphere and surface properties. Crucially, the satellite data employed are not included as observational input into the data assimilation system and therefore provide a truly independent test for the realism of the simulated climate.

[4] Previously, *Yang et al.* [1999] assessed the performance of the radiation budget simulated by the National Centers for Environmental Prediction/National Center for Atmospheric Research (NCEP/NCAR) 40-year reanalysis using satellite data from 1985–1986. In the present study we use observations from multiple satellite instruments and the NCEP/NCAR reanalysis to evaluate the quality of the radiation budget, including water vapor and clouds, simulated by the new European Centre for Medium-Range Weather Forecasts (ECMWF) 40-year Reanalysis (ERA40 [*Simmons and Gibson*, 2000]) over the period 1979–2002.

2. Models and Data

2.1. ERA40

[5] The ERA40 reanalysis runs from 1957 to 2002 and is based on the ECMWF operational three-dimensional variational assimilation system, making comprehensive use of satellite and conventional observations. The model uses 60 vertical levels and a T159 spectral resolution and is based on the ECMWF operational integrated forecast system cycle 23r4 which includes semi-Lagrangian advection and prognostic clouds. The Rapid Radiative Transfer Model [*Mlawer et al.*, 1997] is used for the longwave spectrum and the *Fouquart and Bonnel* [1980] scheme is used for the shortwave spectrum. Further details of the model physics, assimilation system and preliminary validation are described by *Chevallier et al.* [2001] and *Simmons* [2001]. In the present study we use 2.5 × 2.5 degree spatial resolution monthly mean and 6-hour data. The period 1979–2001 is chosen to coincide with the primary satellite era thereby allowing comparisons with satellite data and ensuring greater consistency in the observational input to the assimilation system [*Chevallier et al.*, 2003]. On the basis of analysis of ECMWF model spin-up, it was decided to use the 6-hour forecast fields (also referred to as the background field) rather than longer lead times. Longer lead times did not improve the comparisons with the satellite observations of radiative fluxes and water vapor, and it was assumed that the 0- to 6-hour forecast period would provide the maximum observational input to the reanalysis products chosen for analysis.

2.2. Satellite Data

[6] Measurements of the top of atmosphere radiation budget are utilized from three instruments. From the Earth Radiation Budget Experiment (ERBE), covering the period 1985–1990, we use the scanning radiometer from the Earth Radiation Budget Satellite (ERBS) only (60°S–60°N) to avoid spurious signals relating to changes in the polar orbiting satellites during the ERBE period. The Scanner for Radiation Budget instrument (ScaRaB) provides global coverage during 1994/5 and the Clouds and the Earth's Radiant Energy System (CERES) from the Tropical Rainfall Measurement Mission (TRMM) satellite (CERES/TRMM ERBE-like Edition 2 ES4 data) covers 40°S–40°N for January–August 1998. These data are provided as monthly means on 2.5 × 2.5 degree grids and are intercompared and described by *Wielicki et al.* [2002, and references therein] and *Viollier et al.* [2002, and references therein].

Table 1. Global Annual Means (1979–2001) for ERA40 and NCEP and Estimates From Satellite Observations

	ERA40[a]	NCEP[a]	OBS
OLR, W m^{-2}	244.8 (245.8)	237.4 (237.5)	235[b]
OLRc, W m^{-2}	264.8 (265.1)	268.6 (268.5)	264[b]
ASR, W m^{-2}	237.4 (238.5)	226.1 (226.5)	238[b]
ASRc, W m^{-2}	293.9 (293.9)	287.4 (287.4)	286[b]
NET, W m^{-2}	−7.4 (−7.3)	−11.3 (−11.0)	+3[b]
NETc, W m^{-2}	+29.1 (+28.8)	+18.8 (+18.9)	+22[b]
CWV, kg m^{-2}	24.9 (24.9)	23.9 (23.9)	24.5[c]

[a]Means also calculated for the years covered by the satellite observations (in parentheses).
[b]ERBE (1985–1989).
[c]NVAP (1988–1992).

[7] Also utilized are monthly mean estimates of column-integrated water vapor over the oceans from the Scanning Multichannel Microwave Radiometer (SMMR [*Wentz and Francis*, 1992]) for the period 1979–1984 and from version 4 of the Special Sensor Microwave Imager (SSM/I [*Wentz*, 1997]) for the period 1987–1999. Estimates of total cloud fraction were taken from the International Satellite Cloud Climatology Project (ISCCP [*Rossow and Schiffer*, 1999]) version D2.

2.3. Additional Model and Reanalysis Data

[8] Additionally, we employed monthly mean data from the NCEP/NCAR reanalysis [*Kalnay et al.*, 1996] for the period 1979–2001 and from the Hadley Centre atmospheric climate model, HadAM3, using observed sea surface temperature forcing experiments described by *Allan et al.* [2003] for the period 1979–1998. We also use the NASA Surface Radiation Budget longwave product (release 2) which combines satellite radiance data, data assimilation and radiative transfer models [*Fu et al.*, 1997] to estimate surface and top of atmosphere radiative fluxes.

3. Global Annual Means

[9] Table 1 shows global annual means for top of atmosphere fluxes and column-integrated water vapor (CWV) for ERA40 and NCEP data over the period 1979–2001. OLR is the outgoing longwave radiation, ASR is the net absorbed solar radiation, and NET is the net downward radiation at the top of the atmosphere. The subscript, *c*, denotes the clear-sky flux component. Also displayed are observational estimates from ERBE [*Kiehl et al.*, 1994] and from the NASA Water Vapor Data set (NVAP), which combines conventional and satellite derived water vapor retrievals to produce a global data set of column water vapor [*Randel et al.*, 1996]. In addition, the ERA40 and NCEP means corresponding with the 1985–1989 ERBE data and the 1988–1992 NVAP data are displayed in parentheses. The observational uncertainties for the ERBE data are quoted as ±5 W m^{-2}. Because the NVAP data are derived from multiple sources, it is difficult to estimate the measurement uncertainty; the expected retrieval error of the SSM/I instrument, which is included in the NVAP system, is quoted as 0.6 kg m^{-2} [*Wentz*,

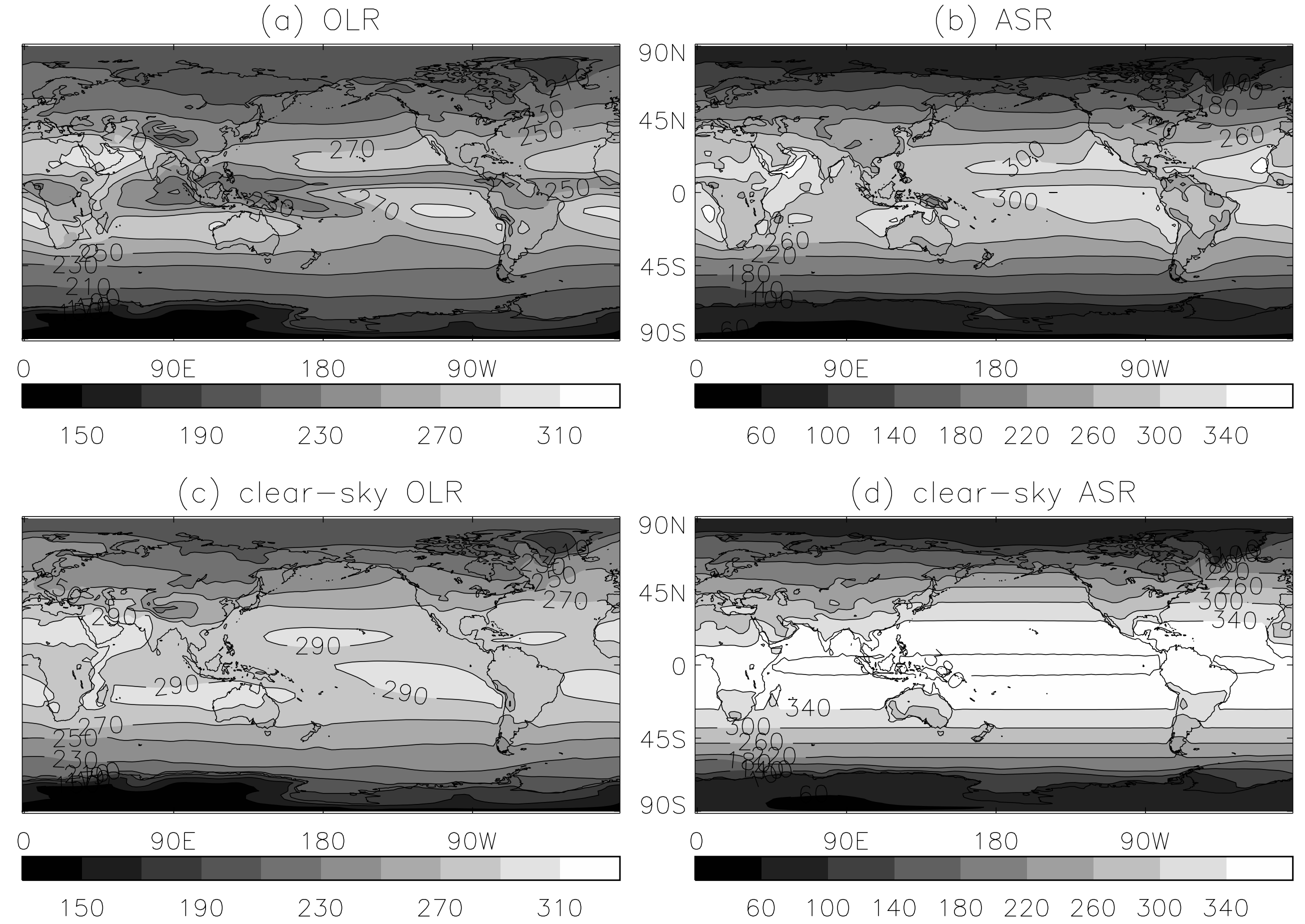

Figure 1. The 1979–2001 means of (a) outgoing longwave radiation (OLR), (b) absorbed solar radiation (ASR), (c) clear-sky OLR, and (d) clear-sky ASR simulated by ERA40 (units W m^{-2}). See color version of this figure in the HTML.

1997]. Clear-sky OLR and water vapor simulated by ERA40 and NCEP are in good agreement with the satellite data. However, ERA40 overestimates OLR and clear-sky ASR, and NCEP underestimates ASR compared to ERBE. While ERBE gives a small positive net radiative imbalance of 3 W m^{-2}, both ERA40 and NCEP simulate net radiative cooling at the top of the atmosphere. Comparisons between ERBE and NCEP are consistent with the findings of *Yang et al.* [1999].

[10] While it is informative to compare the global annual mean energy budget, it is likely that compensating errors are contributing toward the average values. In the following sections we analyze in more detail the regional and temporal structure of the differences between ERA40 and the satellite/NCEP data. As a frame of reference, maps of the 1979–2001 annual mean top of atmosphere radiative energy balance simulated by ERA40 are displayed in Figure 1. These plots show a general increase in absorbed solar radiation and outgoing longwave emission with decreasing latitude. This relates to the increased insolation and resulting higher temperatures at lower latitudes. Additional spatial variability in the clear-sky fluxes results from the surface and atmospheric properties such as surface albedo, surface temperature, and water vapor. The all-sky radiation budget is modified further by the radiative impact of clouds which reduce both the absorbed solar radiation and the outgoing emission of longwave radiation.

4. Clear-Sky Radiation Simulation

[11] Clouds introduce a large uncertainty in the measurement and the simulation of the Earth's radiation budget [e.g., *Wielicki et al.*, 2002]. However, to correctly interpret the cloud radiative effect on the radiation budget, it is first necessary to verify the quality of the clear-sky fluxes. Additionally, careful comparisons between measurements and model estimates of clear-sky irradiance provide substantial diagnostic information on the realism of the atmosphere and surface properties. We first concentrate on assessing the quality of clear-sky fluxes produced by ERA40.

[12] Previously, *Slingo et al.* [1998] produced simulations of clear-sky longwave fluxes and heating rates using the ECMWF 15-year reanalysis (ERA15) as input to a radiation scheme (CLERA). This methodology was necessary because ERA-15 did not produce clear-sky radiation diagnostics. The CLERA simulations were evaluated using ERBE satellite measurements [*Slingo et al.*, 1998] and ground-based measurements [*Allan*, 2000] and used in

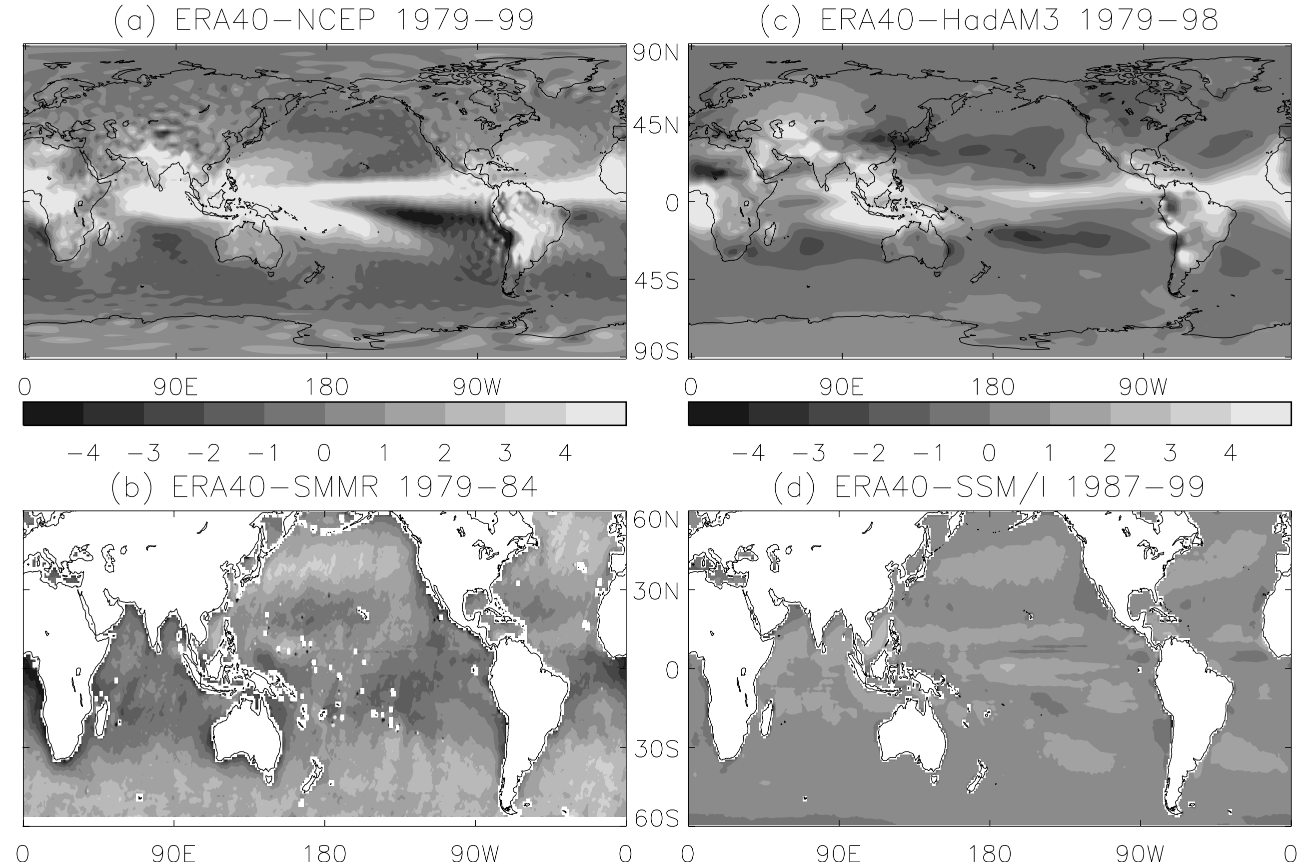

Figure 2. Column-integrated water vapor difference (kg m^{-2}) for (a) ERA40-NCEP, (b) ERA40-SMMR, (c) ERA40-HadAM3, and (d) ERA40-SSM/I. See color version of this figure in the HTML.

studies of water vapor feedback [*Allan et al.*, 1999; *Slingo et al.*, 2000]. For ERA40, clear-sky flux diagnostics were produced directly as part of the reanalysis system. On the basis of analysis of preliminary ERA40 data it was decided that the CLERA simulation methodology was not required to calculate clear-sky longwave radiative fluxes. In addition to the longwave diagnostics, clear-sky shortwave radiative diagnostics are available from ERA40.

[13] Errors in the ERA15 assimilation system caused spurious interannual changes in low-altitude temperature and moisture [e.g., *Trenberth et al.*, 2001; *Allan et al.*, 2002] which are likely to limit the utility of the CLERA data to analyze the subtle global changes in the clear-sky greenhouse effect and water vapor feedback. It is important to scrutinize the quality of water vapor and clear-sky radiation in the new ERA40 products.

4.1. Clear-Sky Surface Downwelling Longwave Radiation and Water Vapor

[14] The global coverage of clear-sky flux measurement is more problematic at the surface than at the top of the atmosphere. While it is possible to estimate surface radiative fluxes from the top of atmosphere radiation [e.g., *Rossow and Zhang*, 1995], this is difficult, particularly for surface downwelling longwave radiation (SDL), which can be highly decoupled from the top of atmosphere fluxes. Because clear-sky SDL is strongly dependent on near-surface temperature and low-level water vapor concentration [e.g., *Gupta*, 1989; *Allan*, 2000], one way to assess the quality of global surface downwelling flux indirectly is to compare satellite estimates of column-integrated water vapor with ERA40. This is possible using satellite microwave radiometers which provide estimates of CWV over the oceans.

[15] Figure 2a shows differences between ERA40 and NCEP data for 1979–2001. Over tropical convective regions, ERA40 simulates over 4 kg m^{-2} more CWV than NCEP, while over descending regions of the tropics, ERA40 simulates lower CWV totals than NCEP. It is interesting to note that a similar CWV difference signal is apparent in the comparison between ERA40 and HadAM3 (Figure 2c [see also *Allan et al.*, 2003]). However, on comparing ERA40 with SMMR satellite data for 1979–1984 (Figure 2b) and SSM/I data for 1987–1999 (Figure 2d) over the oceans, difference distributions are dissimilar to and smaller than the ERA40 minus NCEP or HadAM3 comparisons. Differences between ERA40 and SSM/I are generally slightly positive and of similar magnitude to the expected RMS calibration error of 1.2 kg m^{-2} for SSM/I [*Wentz*, 1997]. Although SSM/I data were assimilated by ERA40, the agreement is excellent considering the differences between the *Wentz* [1997] regression techniques and the ERA40 method, which used 1-D variational assimilation of the data. However, the SMMR data provide a truly independent comparison with ERA40 (Figure 2b) because the SMMR data were not assimilated by ERA40. Here, ERA40 shows agreement to within 1 kg m^{-2} over much of the tropical

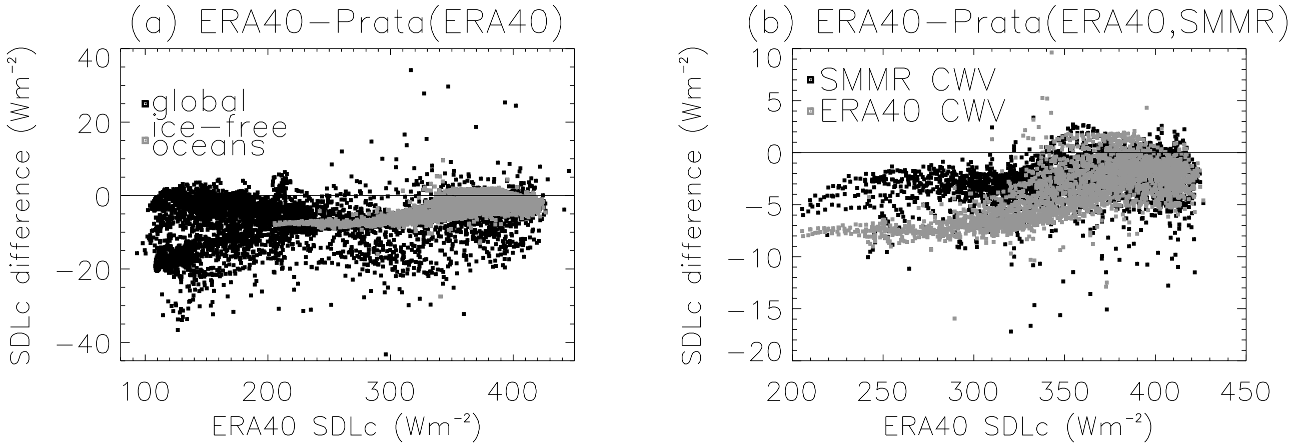

Figure 3. Clear-sky surface downwelling longwave irradiance (SDLc) differences (ERA40 minus Prata formula) for 1979–1984 mean data (a) globally (black) and over ice-free oceans (gray) using ERA40 T_0 and CWV as input to the Prata formula and (b) over ice-free oceans only using ERA40 T_0 and either ERA40 CWV (gray) or SMMR CWV (black) as input to the Prata formula.

oceans. Over midlatitude oceans, ERA40 overestimates moisture by up to 3 kg m^{-2}. *Bengtsson et al.* [2004b] argue that much of the skill in representing the column water vapor in ERA40 results from the realism of the dynamics and its ability to advect water correctly rather than due to the assimilation of water vapor data.

[16] The excellent agreement between ERA40 CWV and the satellite data suggests that surface downwelling longwave fluxes over the oceans are also of high quality. To investigate this further, we now compare clear-sky downwelling longwave radiation at the surface (SDLc) from ERA40 with a simple model based on radiative transfer theory and statistical fits to ground-based radiometric observations [*Prata*, 1996]. The formula uses screen level temperature and specific humidity to predict column-integrated water vapor, which is the primary determinant of atmospheric longwave emissivity. We apply the following form where SDLc is related to CWV and screen level temperature (T_0):

$$\mathrm{SDLc} = \left\{1 - (1+u)\exp\left[-(1.2+3u)^{\frac{1}{2}}\right]\right\}\sigma T_0^4, \qquad (1)$$

where u = 0.1CWV, σ (=5.67 × 10^{-8} W m^{-2} K^{-4}) is the Stefan-Boltzmann constant. When using climatological data, *Prata* [1996] found the formula to produce RMS differences of ±6.0 W m^{-2}. Here we prescribe annual mean column-integrated water vapor using ERA40 values or SMMR values and use 1.5 m air temperatures from ERA40 to prescribe T_0. Because the formula has been developed based on surface radiometric observations, this provides an independent test of the global simulation of SDLc by ERA40.

[17] Figure 3a shows differences in SDLc for ERA40 minus the Prata formula using ERA40 CWV and T_0 as input. Differences are plotted as a function of ERA40 SDLc. Globally, ERA40 tends to underestimate SDLc compared to the formula by around 0–20 W m^{-2}. Differences over the ice-free ocean grid points are smaller (0–10 W m^{-2}) and are shown as grey dots in both Figures 3a and 3b. Also shown in Figure 3b are the ERA40 minus Prata SDLc differences using SMMR CWV as input to the Prata formula. This gives an idea of the impact of CWV errors in ERA40 on the SDLc simulation. For higher SDLc, corresponding to the tropical convective regions, the impact of using observed CWV as input to the Prata formula compared to using ERA40 data is small. At higher latitudes, where ERA40 overestimates CWV compared to SMMR, the SDLc predicted by the formula is increased by only about 5 W m^{-2}, and the ERA40 minus Prata differences, in fact, become smaller.

[18] The above analysis combined with the evaluation of CWV simulated by ERA40 adds confidence to the climatology of SDLc simulated by ERA40. As an additional check on the ERA40 SDLc we compare with NASA surface radiation budget (SRB) data (longwave product, release 2) which combines satellite radiance data, data assimilation and radiative transfer models [*Fu et al.*, 1997] to estimate surface and top of atmosphere radiative fluxes. Figure 4 shows the ERA40 minus SRB clear-sky SDL differences for 1984–1994 to be generally positive but within 5 W m^{-2} over middle latitude oceans. Differences of up to 15 W m^{-2} are

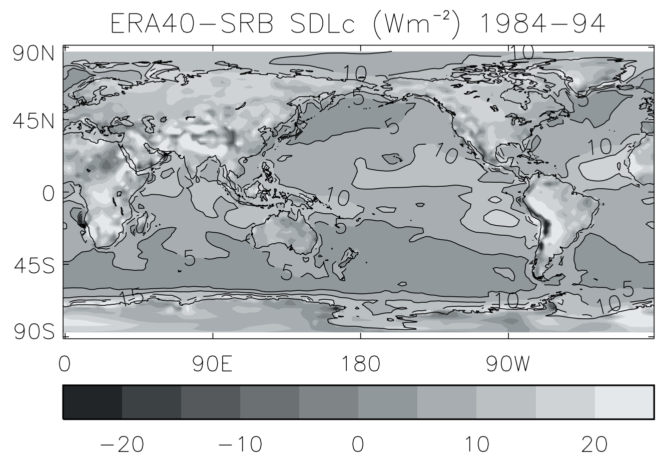

Figure 4. Clear-sky surface downward longwave radiation difference (W m^{-2}) for 1984–1994 (ERA40 minus SRB). Contours are displayed over ocean regions for clarity.

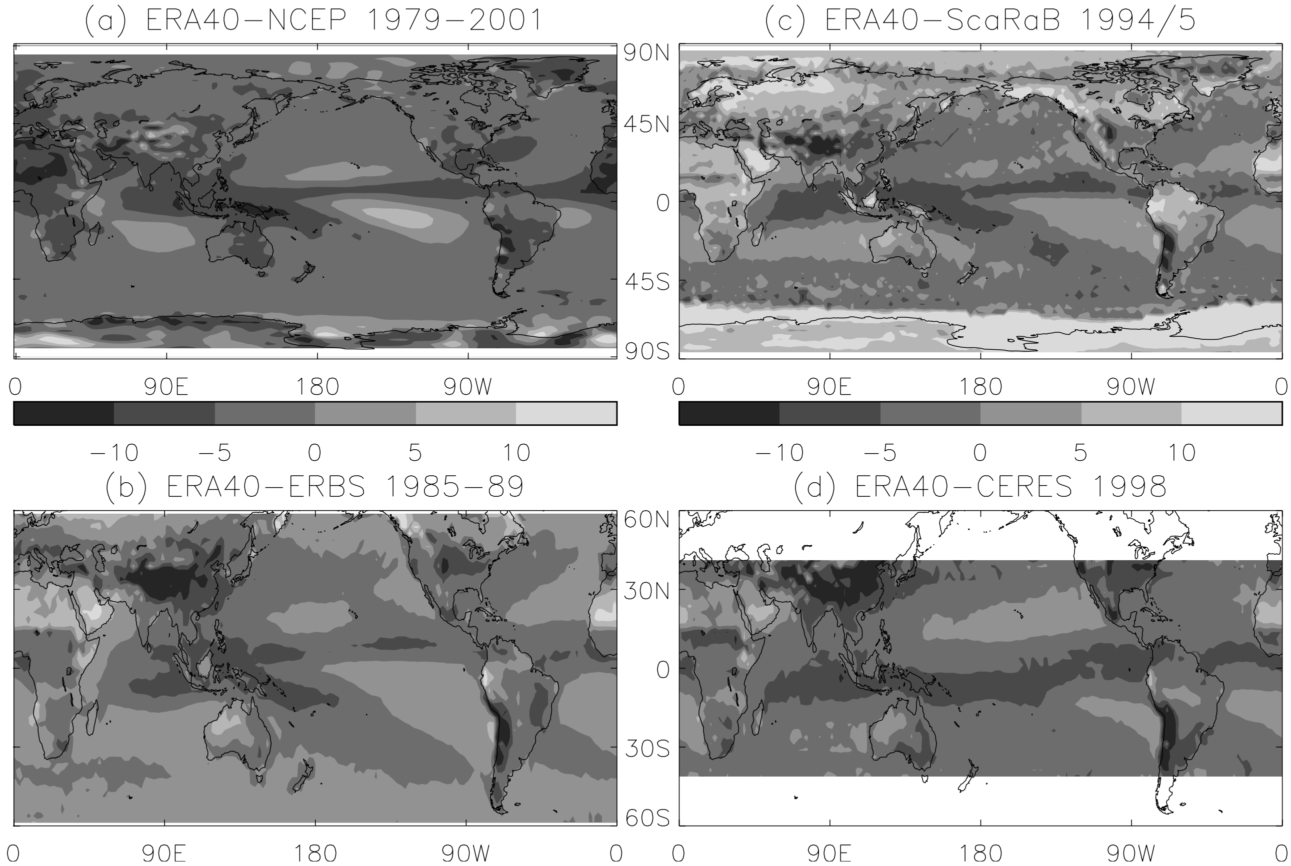

Figure 5. Clear-sky OLR difference (W m^{-2}) for (a) ERA40-NCEP, (b) ERA40-ERBS, (c) ERA40-ScaRaB, and (d) ERA40-CERES. See color version of this figure in the HTML.

present over many land regions and also the marine stratocumulus zones. While previous assessments of the ECMWF model surface longwave fluxes [*Morcrette*, 2002] and clear-sky SDL from ERA15 [*Allan*, 2000] suggest reasonable simulation, further comparisons between ERA40, SRB, and surface radiative flux data are required to confirm the quality of these simulations.

4.2. Clear-Sky OLR

[19] While CWV is an important parameter for determining longwave radiative fluxes near to the surface, longwave radiation at the top of the atmosphere is also strongly dependent on the humidity and temperature away from the boundary layer. Clear-sky OLR comparisons provide therefore additional information on the quality of the reanalysis climate. The climatology of clear-sky OLR simulated by ERA40 is now compared with the NCEP reanalysis and satellite data. Satellite measurements of clear-sky OLR were not used as input to either assimilation system and therefore provide an independent check on the quality of temperature and humidity fields, in addition to the clear-sky greenhouse effect, simulated by ERA40. Figure 5 shows ERA40 clear-sky OLR differences relative to NCEP, ERBS, ScaRaB, and CERES for multiannual means using time-matching data. Over low latitudes, clear-sky OLR differences generally indicate humidity differences of opposite sign, while over higher latitudes, clear-sky OLR differences mainly relate to temperature differences of like sign [e.g., *Allan et al.*, 1999].

[20] ERA40 clear-sky OLR is generally lower than NCEP values apart from over oceanic subtropical subsidence regions (Figure 5a). There is a qualitatively similar pattern to the CWV differences shown in Figure 2a with positive ERA40-NCEP moisture differences corresponding with negative ERA40-NCEP clear-sky OLR differences. Over land, the clear-sky OLR differences between ERA40 and NCEP are generally of opposite sign compared to the ERA40 minus satellite data differences. This is particularly applicable to north Africa, where NCEP simulates about 10 W m^{-2} more clear-sky OLR than ERA40, which in turn simulates up to 15 W m^{-2} more clear-sky OLR compared to the satellite data. *Allan et al.* [2003] also found HadAM3 to overestimate clear-sky OLR compared to ERBS data over this region. For the NCEP data, *Yang et al.* [1999] attributed these differences to overestimations of surface emissivity or temperature. *Slingo et al.* [1998] also found that ERA15 overestimates clear-sky OLR over north Africa and attributed the discrepancy in July to overestimations in ERA15 surface temperature based on comparison with surface observations. However, surface temperature errors could not explain the differences in January.

[21] Over Northern Hemisphere land and over the Antarctic region, ERA40 overestimates clear-sky OLR by more than the nominal ScaRaB accuracy of 5 W m^{-2} (Figure 5c). This primarily affects the Northern Hemisphere winter season (not shown). Differences of opposite sign were found in comparisons between ERA15 and ERBE [*Slingo*

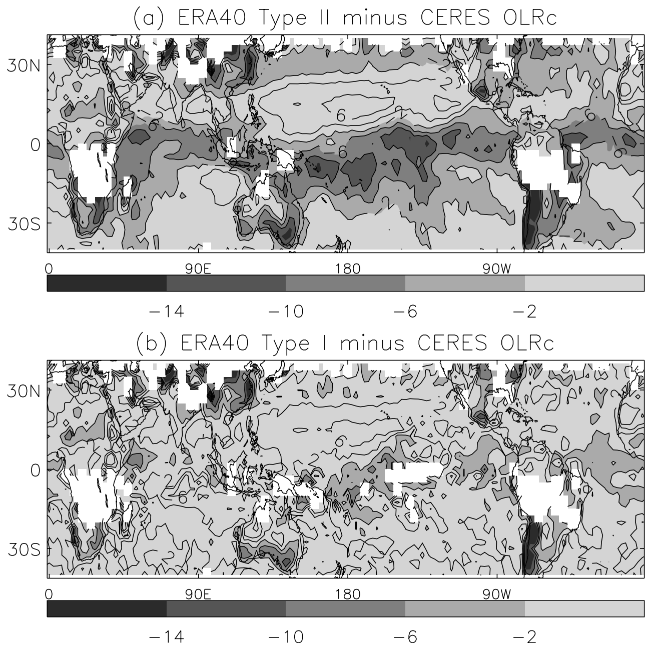

Figure 6. ERA40 minus CERES clear-sky OLR (W m^{-2}) for January 1998 using (a) standard ERA40 "type II" clear-sky diagnostic and (b) applying satellite-like sampling "type I" to ERA40 data. Contour interval is 4 W m^{-2}.

et al., 1998] and these related to underestimations in ERA15 land temperature in winter which have since been improved in ERA40 [*Simmons*, 2001]. It is possible that these corrections have overcompensated the previous negative temperature errors, resulting in overestimates in winter surface temperature over Europe and North America. Surface temperatures in ERA40 are generally higher than NCEP over Northern Hemisphere land, particularly in the winter season (not shown).

[22] Over the oceans, comparisons between ERA40 and the satellite data indicate similar difference fields to the comparison with NCEP [see also *Yang et al.*, 1999]. Intuitively, this suggests that humidity in ERA40 is overestimated over tropical convective regions and underestimated over tropical subsidence regions. Some of the discrepancy may relate to incomplete knowledge of the water vapor continuum and far-infrared absorption [e.g., *Harries*, 1997; *Wong et al.*, 2000]. However, the negative ERA40 minus satellite data clear-sky OLR can also be explained by the inconsistent sampling of clear skies between models and satellite data [*Allan and Ringer*, 2003; *Cess and Potter*, 1987]. In the reanalyses, as in climate models, clear-sky fluxes are calculated diagnostically using the atmospheric profiles of temperature and water vapor at all grid points, regardless of cloud cover. However, the satellite data only measure clear-sky fluxes over cloud-free regions. Because such regions tend to be dry compared to cloudy regions, the satellite clear-sky OLR is biased high compared to the model/reanalysis data. This can be illustrated using 6-hour data from ERA40 as follows.

[23] Figure 6a shows ERA40 minus CERES clear-sky OLR differences for January 1998. Negative differences of order 10 W m^{-2} are observed over the equatorial zone while smaller positive differences are present over the dry, clear zone across the northern Pacific between about 10 and 20°N. In Figure 6b we apply satellite-like sampling to the ERA40 data by removing from the analysis all grid points where cloud fraction is above a threshold of 50%. Although this threshold is rather arbitrary, it is reasonable to assume that within the relatively large ERA40 grid boxes, the smaller satellite pixels will detect some clear-sky scenes. Varying the threshold does not alter the main conclusions of the analysis (for further discussion, see *Allan et al.* [2003]).

[24] Over the dry North Pacific zone, positive clear-sky OLR differences are insensitive to the clear-sky sampling because the low amounts of cloud ensure consistent sampling between the satellite and ERA40 data. However, over the moist equatorial zone, the negative differences between ERA40 and CERES shown in Figure 6a are diminished in Figure 6b, where satellite-like sampling is applied to ERA40. Therefore the negative clear-sky OLR differences shown in Figures 5b–5d can be explained by the sampling inconsistency rather than errors in ERA40 humidity. Further, although NCEP clear-sky OLR appears to agree well with the satellite data over the tropical convective regions, it is possible that a cancellation between satellite sampling inconsistencies and underestimation of atmospheric humidity applies. Indeed, Figure 2 provides evidence that tropical CWV is underestimated by NCEP. However, there is also evidence in Figures 5 and 6 that ERA40 may underestimate humidity over tropical ocean subsidence regions [see also *Allan and Ringer*, 2003].

4.3. Clear-Sky Shortwave Radiation

[25] Figure 7 shows multiannual mean differences between clear-sky ASR simulated by ERA40 and given by temporally coincident data from NCEP, ScaRaB, ERBS, and CERES. In general, ERA40 overestimates the ASRc over Northern Hemisphere land compared to NCEP and ScaRaB, suggesting that ERA40 surface albedos are too low. However, the differences are smaller compared to ERBS. While the surface albedo over high-latitude forests was improved in ERA40 [*Simmons*, 2001], it appears that ERA40 absorbs too much solar radiation for clear skies throughout the year (not shown). Over north Africa, ERA40 overestimates ASRc by more than 15 W m^{-2} compared to the satellite data. This is consistent with the analysis of *Yang et al.* [1999], who showed that NCEP ASRc data are also overestimated compared to ERBE data and attributed the discrepancy to an underestimation in surface albedo.

[26] Over the ocean, ERA40 overestimates ASRc slightly, but differences are comparable to the satellite data accuracy of about 5 W m^{-2}. ERA40 simulates over 10 W m^{-2} more ASRc than NCEP over the equatorial Pacific. Differences between ERA40 and the satellite data are generally smaller than 10 W m^{-2} over this region, indicating that NCEP underestimates ASRc here. Because simple aerosol climatologies are used in ERA40, this may affect the accuracy of simulated ASRc. As is shown in section 4.4, interannual changes in ASRc following volcanic eruptions are also likely to be unrealistic in ERA40.

4.4. Interannual Variability

[27] While the spatial distribution of clear-sky longwave radiative fluxes and water vapor appears well simulated by

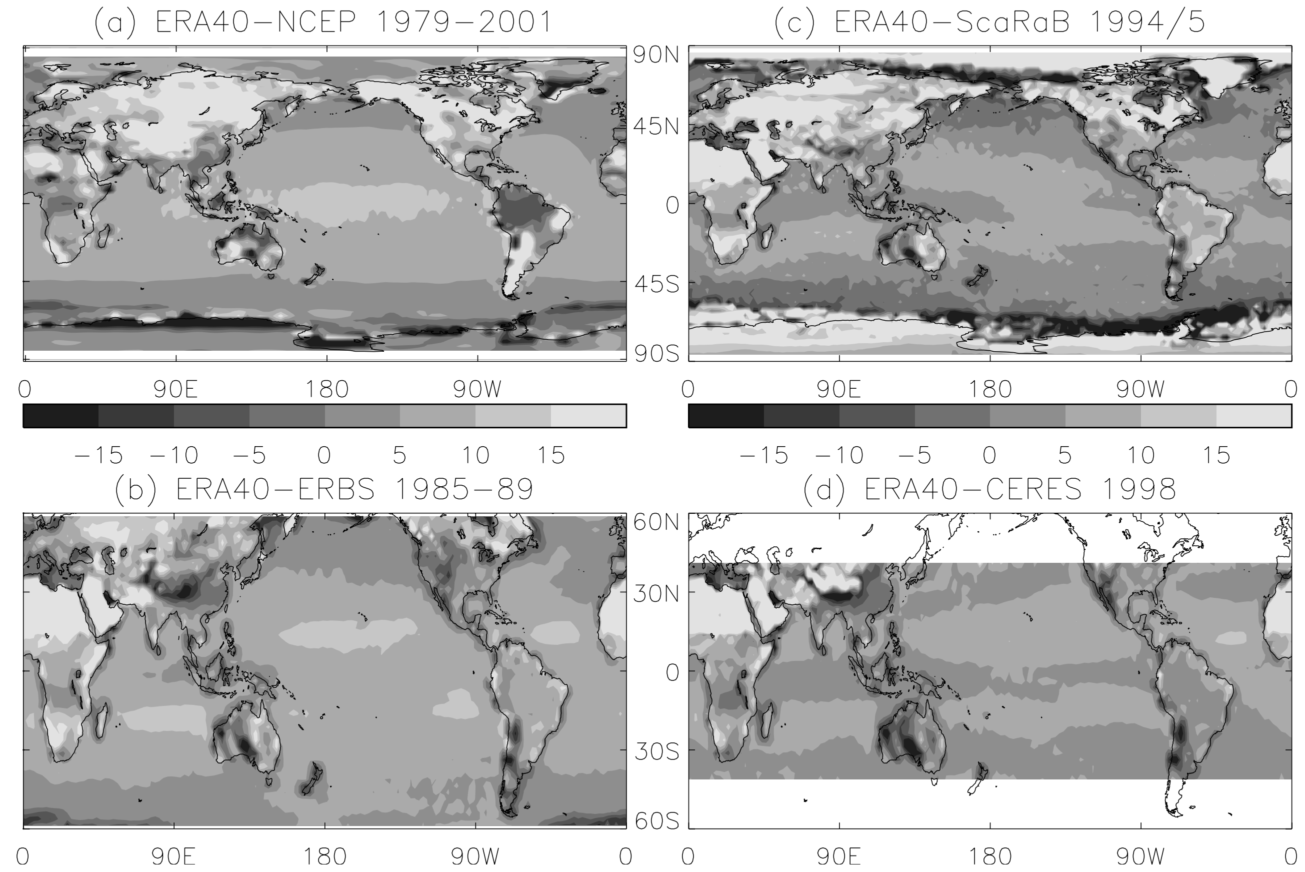

Figure 7. Clear-sky absorbed solar radiation differences (top of atmosphere) (W m^{-2}) for (a) ERA40-NCEP, (b) ERA40-ERBS, (c) ERA40-ScaRaB, and (d) ERA40-CERES. See color version of this figure in the HTML.

ERA40, it is also important to examine the temporal variations. Previously, *Allan et al.* [2002] found that interannual CWV variations in a preliminary version of ERA40 were more realistic than the much larger variations produced by ERA15 when comparing to satellite observations. Spurious changes in water vapor will also impact the accuracy of longwave radiative fluxes. We therefore now compute the interannual variability of CWV in the final ERA40 product and compare this with NCEP, HadAM3, and the satellite data. The low-latitude (40°S–40°N) ocean area-weighted means are first calculated for each month. Subsequently, the mean monthly annual cycles for the reference period 1988–1992 are removed from each data set. The resulting time series are smoothed using a 3-month moving window.

[28] Figure 8 compares the interannual monthly anomalies of CWV. Consistent with the analysis of ERA15 data by *Allan et al.* [2002], the interannual variations of CWV simulated by ERA40 are smaller than for ERA15 and in closer agreement with the SMMR and SSM/I observations. In particular the increases in moisture relating to the 1982/1983 and 1997/1998 El Niño warm events are well captured. However, ERA40 produces negative anomalies of CWV at the beginning of 1980 and during 1987/1988 and positive anomalies in 1992 and 1995 which appear unrealistic compared with the SMMR and SSM/I satellite data. The anomalies during 1991 relate to bias correction errors in the assimilation system introduced following the Pinatubo volcanic eruption and the 1995 anomalies are likely to relate to erroneous assimilation of High-Resolution Infrared Sounder (HIRS) observations during this period. Interannual anomalies of CWV produced by NCEP are in closer agreement with the satellite data than the ERA40 data, although NCEP does not capture the increasing water vapor trend. It is important to note that the CWV simulated by HadAM3 forced with observed sea surface temperatures is in even better agreement with the satellite observations [see also *Allan et al.*, 2003]. Increasing the forecast lead time reduces the errors in interannual variability of water vapor (A. Simmons, personal communication, 2003). However, at longer forecast lead times, influence of the data assimilation on the ECMWF model becomes progressively smaller. This merely emphasizes that errors and changes in the reanalysis observational input are likely to produce erroneous interannual changes in large area-mean changes in water vapor. In agreement with *Bengtsson et al.* [2004a], this suggests that reanalyses are not yet of high enough quality to study the subtle signals of decadal changes in water vapor and water vapor feedback.

[29] A similar analysis of interannual variability was performed on the clear-sky OLR data from ERA40, NCEP, ERBS, ScaRaB, and CERES over low latitude regions (land and ocean). Interannual anomalies were calculated relative to the mean seasonal cycle over the reference period 1985–

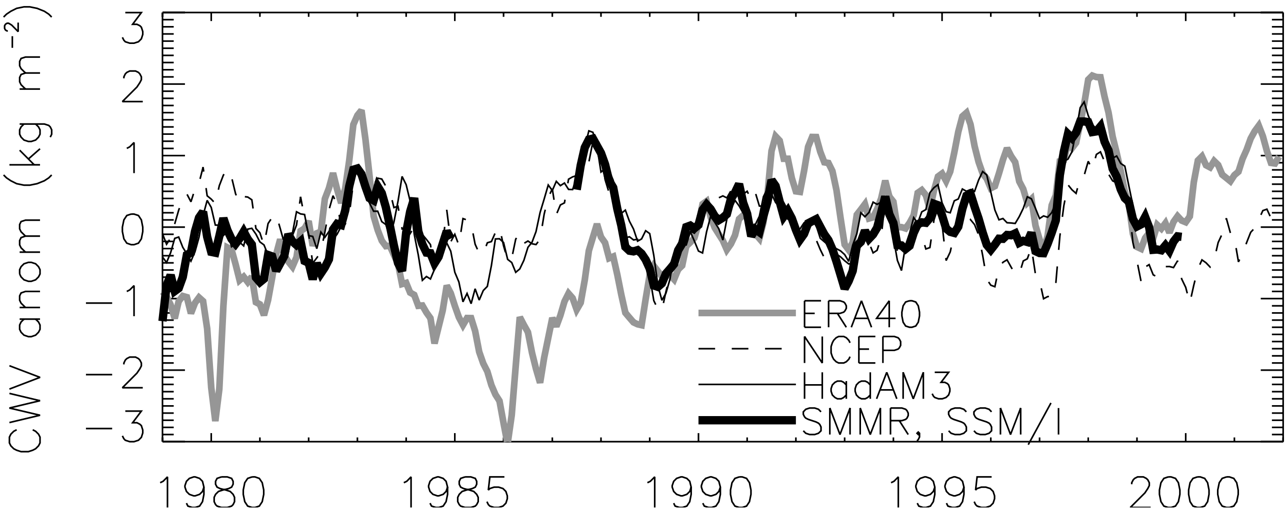

Figure 8. Interannual monthly anomalies of column-integrated water vapor (kg m^{-2}) for ERA40, NCEP, HadAM3, SMMR, and SSM/I over low-latitude (40°S–40°N) oceans.

1989. Figure 9 shows interannual anomalies of clear-sky OLR from HadAM3 and NCEP to be in reasonable agreement with each other and also with the independent satellite observations. While ERA40 also displays good agreement for much of the time series, negative anomalies are apparent for 1981–1985 and from 1997 onward. In agreement with the analysis of column water vapor, this suggests that interannual variability of large-area means of clear-sky OLR, and therefore humidity, in ERA40 are not of high enough quality to provide useful information on water vapor trends and feedback.

[30] *Allan et al.* [2003] showed that while the clear-sky sampling differences between models and satellite data do not appear to affect the interannual variations of clear-sky OLR, accurate changes in greenhouse gas and volcanic aerosol concentrations are required to correctly represent interannual changes in low-latitude mean clear-sky OLR. Volcanic aerosol also strongly affects the absorbed solar radiation as is demonstrated in Figure 10. Here we show interannual monthly anomalies of ASRc for ERA40 and two versions of HadAM3 described by *Allan et al.* [2003]. Both ERA40 and HadAM3 with sea surface temperature (SST) forcing show only little variation in ASRc over the 1979–1998 period. However, when volcanic aerosols are included in the HadAM3 experiment, large negative anomalies of ASRc relating to the El Chichon and Pinatubo eruptions are evident. Thus ERA40 will overestimate ASRc in the years following these eruptions.

5. All-Sky Radiation and Cloud Cover

[31] Although cloud parameters are not assimilated by ERA40, the fundamental link between clouds and climate ensures that availability of such products from ERA40 is potentially of considerable value in a variety of applications. Having established that the climatology of clear-sky

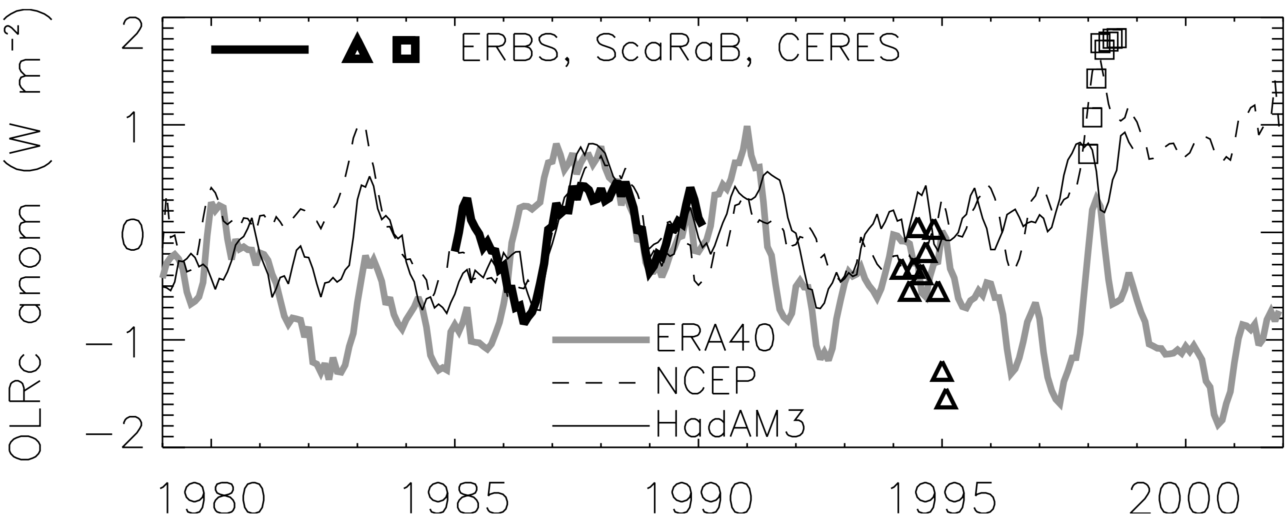

Figure 9. Interannual monthly anomalies of clear-sky outgoing longwave radiation (W m^{-2}) for ERA40, NCEP, HadAM3, ERBS, ScaRaB, and CERES over low-latitude regions (40°S–40°N).

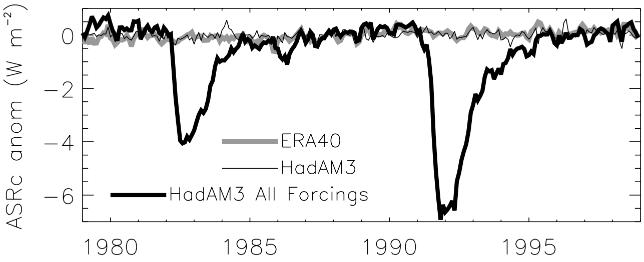

Figure 10. Global interannual monthly anomalies of clear-sky absorbed solar radiation (W m^{-2}) for ERA40, HadAM3 with SST forcing only, and HadAM3 with additional forcings including volcanic aerosols. The all forcing HadAM3 anomalies are normalized with respect to the 1986–1990 period.

radiation simulated by ERA40 is of reasonable quality, we now make assessment of the total radiation budget at the top of the atmosphere which includes the radiative contribution of clouds. Figure 11 shows zonal mean differences for ERA40 minus temporally consistent satellite or NCEP data. ERA40 overestimates OLR by up to 15 W m^{-2} compared to the satellite data, consistent with the 10 W m^{-2} overestimation in the global mean shown in Table 1. Geographically, this discrepancy is apparent over much of the globe, with the largest overestimation (more than 20 W m^{-2}) occurring over tropical land (not shown). The general overestimation in OLR over midlatitude oceans is consistent with an underestimation in cloud top altitude in ERA40 identified by *Chevallier et al.* [2001]. Smaller OLR differences occur over tropical oceans. ERA40 underestimates OLR over some tropical ocean regions compared to CERES data in 1998. This may relate to the apparent decadal increases in OLR observed over the tropics between 1985 and 2000 [*Wielicki et al.*, 2002] which remain to be confirmed. Nevertheless, over tropical regions, there is some degree of compensation between an overestimation in high cloud fraction and an underestimation in the frequency of very cold cloud tops [*Chevallier et al.*, 2001]. In the extra tropics, *Chevallier et al.* [2003] identified an underestimation in cloud ice water which is also consistent with unrealistically high OLR simulated by ERA40.

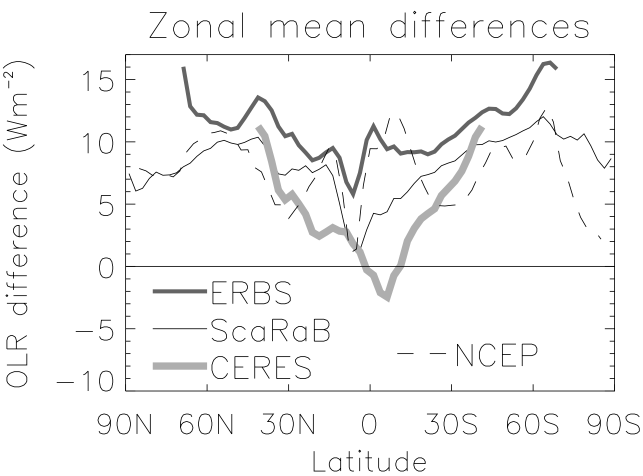

Figure 11. Zonal mean OLR differences for ERA40 minus ERBS, ScaRaB, CERES, and NCEP.

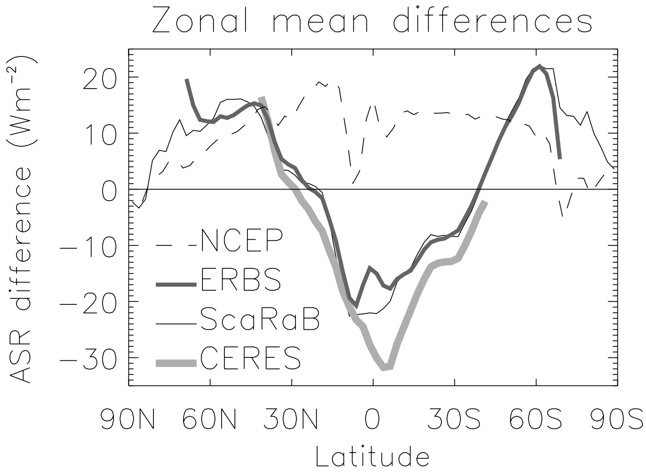

Figure 12. Zonal mean ASR differences for ERA40 minus ERBS, ScaRaB, CERES, and NCEP.

[32] Figure 12 shows zonal mean ASR differences between ERA40 and time-matching data from NCEP, ERBS, ScaRaB, and CERES. Again, each line denotes ERA40 minus the comparison data set. Despite the good agreement in the global annual mean of ASR between ERA40 and ERBE observations, the zonal mean differences show that this results from a compensation between underestimations in ASR in the tropics and overestimation in ASR in the extratropics by ERA40. ERA40 underestimates ASR over tropical regions by up to 30 W m^{-2} compared to the satellite data. This underestimate operates across the entire tropics apart from over north Africa and over marine stratocumulus regions where ERA40 overestimates ASR by more than 30 W m^{-2} (not shown). NCEP ASR is also underestimated compared to the satellite data, in agreement with *Yang et al.* [1999], although NCEP simulates more realistic ASR over the marine stratocumulus regions. Over higher latitudes, ERA40 tends to overestimate ASR compared to the satellite data and NCEP. The overestimation in ASR over north Africa and high-latitude land is explained by the clear-sky component as shown previously in Figure 7 and relating to surface errors in ERA40 and NCEP [*Yang et al.*, 1999]. Further analysis of the distribution of ASR simulated by ERA40 suggests that deep tropical clouds are too reflective, low-level clouds over the ocean are too frequent, and the radiative effect of stratocumulus clouds is severely underestimated by ERA40 consistent with *Chevallier et al.* [2001].

[33] Comparing cloud fraction simulated by ERA40 and estimated by ISCCP satellite data for 1983–1993 (Figure 13) clearly shows underestimation of cloud fraction by ERA40 over marine stratocumulus regions consistent with the unrealistic radiation budget over these regions. Away from the equatorial zone, clouds appear to be underestimated over ocean regions. This is inconsistent with the overestimation in shortwave cloud radiative effect over these regions. However, ISCCP cloud fraction also contains significant errors due to lack of account for limb effects; for example, the cloud fraction difference structure over the Indian Ocean

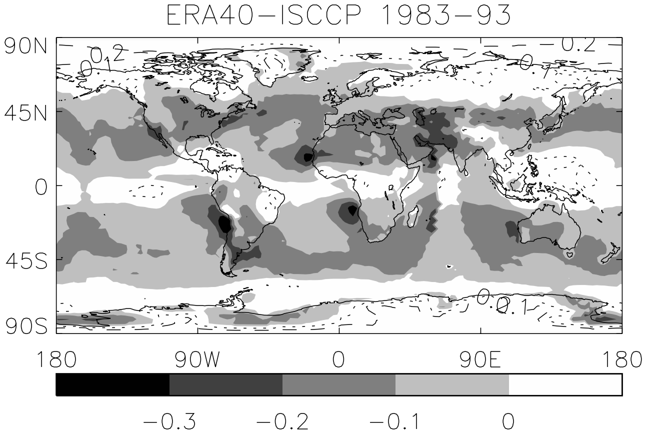

Figure 13. ERA40 minus ISCCP differences of total cloud cover (1983–1993). Shading denotes negative differences while positive difference contours are denoted by dots (+0.1) and dashes (+0.2).

in Figure 13 relates to the edges of the Meteosat and GMS geostationary satellites used by ISCCP. There is also the possibility of instrument calibration issues since there is no visible channel calibration source on the ISCCP satellites. Notwithstanding these errors, Figures 11–13 show a consistent latitudinal signal of cloud radiative effect in ERA40: At low latitudes, there is a tendency for ERA40 to display positive cloud fraction differences which are consistent with OLR and ASR differences becoming more negative (increased cloud radiative effect). This is likely to relate to the overestimation of high cloud fraction in the tropics identified by *Chevallier et al.* [2001] for preliminary ERA40 data. Overall, the total-sky radiation budget simulated by ERA40 displays large systematic biases and is generally inferior to the NCEP total-sky radiation budget which itself has serious limitations. *Yang et al.* [1999] relate these limitations to possible shortcomings in the cloud/moisture parameterizations in the NCEP assimilations systems. In ERA40, the distribution of cloud and its variation in response to sea surface temperature changes appear reasonable. For example, Figure 14 shows that ERA40 captures the interannual changes in cloud fraction observed by ISCCP over the central Pacific (180–190°E, 5°S–5°N). This suggests that it is generally the radiative properties of the cloud, rather than the cloud fraction, which explain the shortcomings in the radiation budget in ERA40.

6. Conclusions

[34] In this paper we assess clouds, water vapor, and the radiative energy budget simulated by the ECMWF 40-year reanalysis (ERA40) over the period 1979–2001 utilizing multiple satellite instruments and the NCEP/NCAR reanalysis. We find that the top of atmosphere radiation budget is poorly simulated by ERA40 and inferior to the NCEP data. This shortcoming is thought to relate to the inaccurate properties of cloud [*Chevallier et al.*, 2001] rather than cloud fraction which shows a reasonable simulation. However, underestimates in cloud fraction over marine stratocumulus regions are responsible for overestimates in ASR in these regions. Also, overestimates in ASR and OLR over north Africa and high-latitude land regions are explained by the clear-sky component and may be related to underestimation of surface albedo by ERA40. Similar findings were presented by *Yang et al.* [1999] for the NCEP reanalysis.

[35] The observed climatology of clear-sky fluxes is well captured by ERA40 over much of the globe. Clear-sky OLR over convective ocean regions is lower in ERA40 than the satellite and NCEP data by about 10 W m^{-2}. However, when the satellite sampling of clear skies is approximated, these differences reduce substantially suggesting that clear-sky OLR is, in fact, well simulated over these regions by ERA40. Further, the small differences in clear-sky OLR between NCEP and ERBE presented by *Yang et al.* [1999] could result from a compensation between a negative bias relating to the different clear-sky sampling and a positive bias due to underestimations in NCEP moisture. Indeed, NCEP is shown to underestimate CWV compared to ERA40 and the satellite data. There is evidence to suggest that ERA40 is too dry over subtropical ocean regions based on overestimations in clear-sky OLR. However, the general quality of clear-sky OLR appears high in ERA40, suggesting considerable possibilities for application in the analysis of climate. For example, *Allan and Ringer* [2003] proposed the use of ERA40 clear-sky OLR and dynamical fields with satellite data to improve the interpretation of longwave cloud radiative forcing.

[36] Differences between ERA40 and satellite estimates of column-integrated water vapor over the oceans are small, generally being between −1 and 3 kg m^{-2} in the multiannual means. The ERA40 simulation appears significantly better than the NCEP reanalysis and HadAM3 climate model which overestimate CWV by more than 4 kg m^{-2} over the tropics [*Allan et al.*, 2003]. *Bengtsson et al.* [2004b] argue that rather than the assimilation of water vapor by reanalyses being responsible for the realistic simulation of column water vapor, good representation of the dynamics is key to the correct representation of water vapor distribution. In the present study we show that ERA40 differences with SSM/I data, which were assimilated by ERA40, are smaller than the differences between ERA40 and SMMR, which were not assimilated by ERA40, suggesting that the water vapor assimilation does contribute to the accuracy of moisture distribution. However, multiannual mean differences between ERA40 and SMMR are less than 3 kg m^{-2}, suggesting that the dynamics operating within ERA40 are of sufficiently high skill to advect water vapor realistically. Indeed, recent studies have shown the power of using dynamical products from reanalyses [*Bony et al.*, 2004] including those from ERA40 [*Allan and Ringer*,

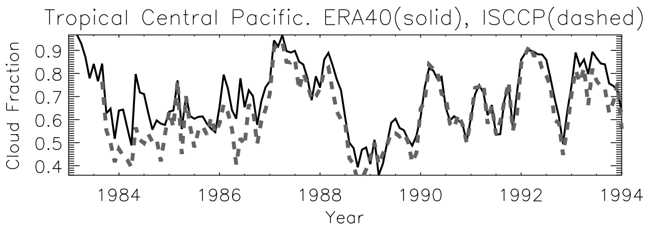

Figure 14. ERA40 and ISCCP cloud fraction over the tropical central Pacific 1983–1993.

2003; *Ringer and Allan*, 2004] along with observations of the radiation budget to analyze changes in cloud and clear-sky forcing of the radiation budget.

[37] One aspect of ERA40 that appears limited is the ability to simulate accurately the subtle interannual and decadal changes of large-area mean parameters such as clear-sky radiation and water vapor. In part, this is due to the large changes in the availability and quality of observations used in the assimilation system. Indeed, it should be noted that providing accurate measurements of global changes in clouds and water vapor presents an enormous challenge for the observational network [*Wielicki et al.*, 2002]. Interannual changes in low-latitude water vapor, although improved over the previous ERA15 system [*Allan et al.*, 2002], still exhibit spurious variability compared to satellite data and are inferior to the variability given by NCEP. However, the water vapor variability simulated by the HadAM3 climate model forced with observed sea surface temperatures reproduces the observed variability more convincingly still than NCEP [*Allan et al.*, 2003]. Similarly, clear-sky OLR variability simulated by ERA40 appears inferior to HadAM3 simulations. This suggests that by careful comparison of observations with carefully controlled climate model experiments, information on water vapor feedback may be more forthcoming [e.g., *Soden et al.*, 2002] in preference to using reanalyses for this purpose. The power of reanalysis products currently available is in their ability to simulate the climatological and synoptic distributions of weather systems over time and space, including the temperature and dynamical fields, and their combination with observational products to evaluate and improve our understanding of the climate system. Only with carefully controlled assimilation experiments involving selection of the most accurate and stable observational input can the subtle variations and trends relating to climate feedbacks be analyzed usefully. At present, some important aspects of the hydrological cycle in reanalyses are not yet good enough for this purpose.

[38] **Acknowledgments.** Sincere thanks to the ERA40 team, especially Adrian Simmons and Sakari Uppala. This work was partially funded through the European Commission contract EVK2-CT-1999-00027 and the NERC/Met Office Connect-B grant NER/D/S/2002/00412 and the UK Department for Environment, Food and Rural Affairs under contract PECD 7/12/37. The ERBE, CERES, SMMR, and SRB data were retrieved from the NASA Langley DAAC, the ScaRaB data were retrieved from the Centre Spatial de Toulouse, and the SSM/I data were retrieved from http://www.ssmi.com/. The NCEP data were retrieved from the NOAA/CIRES Climate Diagnostics Center, and the ERA40 data were provided by ECMWF data services. Three anonymous reviewers are thanked for their constructive comments and suggestions.

References

Allan, R. P. (2000), Evaluation of simulated clear-sky longwave irradiance at the surface using ground-based radiometric observations, *J. Clim.*, *13*, 1951–1964.

Allan, R. P., and M. A. Ringer (2003), Inconsistencies between satellite estimates of longwave cloud forcing and dynamical fields from reanalyses, *Geophys. Res. Lett.*, *30*(9), 1491, doi:10.1029/2003GL017019.

Allan, R. P., K. P. Shine, A. Slingo, and J. A. Pamment (1999), The dependence of clear-sky outgoing long-wave radiation on surface temperature and humidity, *Q. J. R. Meteorol. Soc.*, *125*, 2103–2126.

Allan, R. P., A. Slingo, and V. Ramaswamy (2002), Analysis of moisture variability in the European Centre for Medium-Range Weather Forecasts 15-year reanalysis over the tropical oceans, *J. Geophys. Res.*, *107*(D15), 4230, doi:10.1029/2001JD001132.

Allan, R. P., M. A. Ringer, and A. Slingo (2003), Evaluation of moisture in the Hadley Centre climate model using simulations of HIRS water-vapour channel radiances, *Q. J. R. Meteorol. Soc.*, *129*, 3371–3389.

Bengtsson, L., S. Hagemann, and K. Hodges (2004a), Can climate trends be calculated from reanalysis data?, *J. Geophys. Res.*, *109*, D11111, doi:10.1029/2004JD004536.

Bengtsson, L., K. Hodges, and S. Hagemann (2004b), Sensitivity of large-scale atmospheric analyses to humidity observations and its impact on the global water cycle and tropical and extratropical weather systems in ERA-40, *Tellus*, *Ser. A*, *56*, 202–217.

Bony, S., J.-L. Dufresne, H. Le Treut, J. J. Morcrette, and C. A. Senior (2004), On dynamical and thermodynamic components of cloud changes, *Clim. Dyn.*, *22*, 71–86.

Cess, R. D., and G. L. Potter (1987), Exploratory studies of cloud radiative forcing with a general circulation model, *Tellus*, *39*, 460–473.

Chevallier, F., P. Bauer, G. Kelly, C. Jakob, and T. McNally (2001), Model clouds over oceans as seen from space: comparison with HIRS/2 and MSU radiances, *J. Clim.*, *14*, 4216–4229.

Chevallier, F., G. Kelly, A. J. Simmons, S. Uppala, and A. Hernandez (2003), High clouds over oceans in the ECMWF 15-year and 45-year re-analyses, *ERA40 Proj. Rep. Ser. 11*, 30 pp., Eur. Cent. for Med.-Range Weather Forecasts, Reading, U.K.

Fouquart, Y., and B. Bonnel (1980), Computation of solar heating of the Earth's atmosphere: A new parameterization, *Beitr. Phys. Atmos.*, *53*, 35–62.

Fu, Q., K. N. Liou, M. C. Cribb, T. P. Charlock, and A. Grossman (1997), Multiple scattering parameterization in thermal infrared radiative transfer, *J. Atmos. Sci.*, *54*, 2799–2812.

Gupta, S. K. (1989), A parameterization for longwave surface radiation from sun-synchronous satellite data, *J. Clim.*, *2*, 305–320.

Harries, J. E. (1997), Atmospheric radiation and atmospheric humidity, *Q. J. R. Meteorol. Soc.*, *123*, 2173–2186.

Hartmann, D. L., L. A. Moy, and Q. Fu (2001), Tropical convection and the energy balance at the top of the atmosphere, *J. Clim.*, *14*, 4495–4511.

Kalnay, E. M., et al. (1996), The NCEP/NCAR 40-year reanalysis project, *Bull. Am. Meteorol. Soc.*, *77*, 437–471.

Kiehl, J. T., J. J. Hack, and B. P. Briegleb (1994), The simulated Earth radiation budget of the National Centre for Atmospheric Research community climate model CCM2 and comparisons with the Earth Radiation Budget Experiment (ERBE), *J. Geophys. Res.*, *99*, 20,815–20,827.

Mlawer, E. J., S. J. Taubman, P. D. Brown, M. J. Iacono, and S. A. Clough (1997), Radiative transfer for inhomogenous atmospheres: RRTM, a validated correlated-k model for the longwave, *J. Geophys. Res.*, *102*, 16,663–16,682.

Morcrette, J.-J. (2002), The surface downwelling longwave radiation in the ECMWF forecast system, *J. Clim.*, *15*, 1875–1892.

Prata, A. J. (1996), A new long-wave formula for estimating downward clear-sky radiation at the surface, *Q. J. R. Meteorol. Soc.*, *122*, 1127–1151.

Randel, D. L., T. H. Vonder Haar, M. A. Ringerud, G. L. Stephens, T. J. Greenwald, and C. L. Combs (1996), A new global water vapor dataset, *Bull. Am. Meteorol. Soc.*, *77*, 1233–1246.

Ringer, M. A., and R. P. Allan (2004), Evaluating climate model simulations of tropical cloud, *Tellus*, *Ser. A*, *56*, 308–327.

Rossow, W. B., and R. A. Schiffer (1999), Advances in understanding clouds from ISCCP, *Bull. Am. Meteorol. Soc.*, *80*, 2261–2287.

Rossow, W. B., and Y.-C. Zhang (1995), Calculation of surface and top of atmosphere radiative fluxes from physical quantities based on ISCCP data sets: 2. Validation and first results, *J. Geophys. Res.*, *100*, 1167–1197.

Simmons, A. J. (Ed.) (2001), Workshop on reanalysis, *ECMWF Rep. Ser. 3*, 443 pp., Eur. Cent. for Med.-Range Weather Forecasts, Reading, U.K.

Simmons, A. J., , and J. K. Gibson (Eds.) (2000), The ERA40 Project plan, *ECMWF Rep. Ser. 1*, 62 pp., Eur. Cent. for Med.-Range Weather Forecasts, Reading, U.K.

Slingo, A., J. A. Pamment, and M. J. Webb (1998), A 15-year simulation of the clear-sky greenhouse effect using the ECMWF Reanalysis: Fluxes and comparisons with ERBE, *J. Clim.*, *11*, 690–708.

Slingo, A., J. A. Pamment, R. P. Allan, and P. S. Wilson (2000), Water vapor feedbacks in the ECMWF re-analyses and Hadley Centre climate model, *J. Clim.*, *13*, 3080–3098.

Soden, B. J., R. T. Wetherald, G. L. Stenchikov, and A. Robock (2002), Global cooling after the eruption of Mount Pinatubo: A test of climate feedback by water vapor, *Science*, *296*, 727–730.

Trenberth, K. E., D. P. Stepaniak, and J. W. Hurrell (2001), Quality of Reanalyses in the tropics, *J. Clim.*, *14*, 1499–1510.

Viollier, M., C. Standfuss, and F. Parol (2002), Monthly means of reflected solar flux from POLDER (ADEOS-1) and comparison with

ERBE, ScaRaB and CERES, *Geophys. Res. Lett.*, *29*(10), 1503, doi:10.1029/2001GL014255.

Wentz, F. J. (1997), A well-calibrated ocean algorithm for SSM/I, *J. Geophys. Res.*, *102*, 8703–8718.

Wentz, F. J., and E. A. Francis (1992), Nimbus-7 SMMR ocean products 1979–1984, *Remote Sens. Syst. Tech. Rep. 033192*, 36 pp., Remote Sens. Syst., Santa Rosa, Calif.

Wielicki, B. A., et al. (2002), Evidence for large decadal variability in the tropical mean radiative energy budget, *Science*, *295*, 841–844.

Wong, T., D. F. Young, M. Haeffelin, and S. Weckmann (2000), Validation of the CERES/TRMM ERBE-Like monthly mean clear-sky longwave dataset and the effects of the 1998 ENSO event, *J. Clim.*, *13*, 4256–4267.

Yang, S.-K., Y.-T. Hou, A. J. Miller, and K. A. Campana (1999), Evaluation of the Earth Radiation Budget in the NCEP-NCAR Reanalysis with ERBE, *J. Clim.*, *12*, 477–493.

R. P. Allan and A. Slingo, Environmental Systems Science Centre, University of Reading, Harry Pitt Building, P.O. Box 238, Reading, RG6 6AL, UK. (rpa@mail.nerc-essc.ac.uk; as@mail.nerc-essc.ac.uk)

J. A. Pamment, British Atmospheric Data Centre, Space Science and Technology Department, Rutherford Appleton Laboratory, Fermi Avenue, Chilton Oxfordshire, OX11 0QX, UK. (j.a.pamment@rl.ac.uk)

M. A. Ringer, Met Office, Hadley Centre for Climate Prediction and Research, FitzRoy Road, Exeter, Devon, EX1 3PB, UK. (mark.ringer@metoffice.com)